

# Crystal Nucleation and Growth of Inorganic Ionic Materials from Aqueous Solution: Selected Recent Developments, and Implications

Denis Gebauer,\* Julian D. Gale,\* and Helmut Cölfen\*

In this review article, selected, latest theoretical, and experimental developments in the field of nucleation and crystal growth of inorganic materials from aqueous solution are highlighted, with a focus on literature after 2015 and on non-classical pathways. A key point is to emphasize the so far underappreciated role of water and solvent entropy in crystallization at all stages from solution speciation through to the final crystal. While drawing on examples from current inorganic materials where non-classical behavior has been proposed, the potential of these approaches to be adapted to a wide-range of systems is also discussed, while considering the broader implications of the current re-assessment of pathways for crystallization. Various techniques that are suitable for the exploration of crystallization pathways in aqueous solution, from nucleation to crystal growth are summarized, and a flow chart for the assignment of specific theories based on experimental observations is proposed.

and beyond. Their mechanistic understanding is a prerequisite for controlling, for example, particle size, morphology, and polymorphism. However, quantitative theoretical frameworks for describing and predicting nucleation and growth processes in a holistic manner do not (yet) seem to exist. The role of the solvent is also a critical factor since it determines the thermodynamic competition between solvation and species association, as well as the kinetics often being influenced by the rate of solvent exchange. While a wide range of solvents from organics to ionic liquids can be effective as a crystallization environment, here we will restrict the focus to water as one of the most ubiquitous solvents in environmental and biological processes, while also representing the case of a solvent with strong interactions,

acid-base chemistry, and high dielectric screening.

In recent years, it has become evident that there is a multitude of different pathways from dissolved monomeric constituents to crystals, which can be coarsely subdivided into “classical” and “non-classical” mechanisms.<sup>[1]</sup> While the former assumes that nucleation and growth occur through addition of monomeric species to nuclei and seeds, respectively, “non-classical” frameworks consider a larger range of entities—ranging from clusters, to liquid (nano)droplets and/or (nano)particles—as the relevant species. Much—but certainly not all—of the seminal work on nucleation and crystallization mechanisms has been published by the authors of ref. [1].

Classical nucleation theory (CNT) addresses the dilemma of high pathway complexity using simplification, and assumes that the answer to the nucleation problem can be reduced to basic physical characteristics of nuclei in solution, that is, their surface and bulk-free energies,<sup>[2]</sup> and thereby is often viewed as being universal (for a critical review, see ref. [3]). The historic formulation of CNT is based on the so-called capillary assumption (that is, nanoscopic nuclei are assumed to behave as if they were macroscopic, which is a drastic oversimplification) and the traditional thermodynamics of phase coexistence. Since the pseudo-equilibrium CNT-approach to nucleus formation essentially yields the same expression as, for example, classical density functional theory (CDFT), at least at low levels of supersaturation,<sup>[4]</sup> it is fair to assume that this notion can be used to illustrate the thermodynamic consequences associated with metastable phase fluctuations (Section 1.1), which, in our opinion, can hardly be detected experimentally.


## 1. Introduction

Nucleation, that is, the onset of phase separation in a system that has become supersaturated, and crystal growth processes are of fundamental importance in materials chemistry

D. Gebauer  
Leibniz University Hannover  
Institute of Inorganic Chemistry  
Callinstr. 9, 30167 Hannover, Germany  
E-mail: gebauer@acc.uni-hannover.de

J. D. Gale  
Curtin Institute for Computation/The Institute for Geoscience Research (TiGER)  
School of Molecular and Life Sciences  
Curtin University  
PO Box U1987, Perth, Western Australia 6845, Australia  
E-mail: j.gale@curtin.edu.au

H. Cölfen  
University of Konstanz  
Physical Chemistry  
Universitätsstr. 10, 78465 Konstanz, Germany  
E-mail: helmut.coelfen@uni-konstanz.de

 The ORCID identification number(s) for the author(s) of this article can be found under <https://doi.org/10.1002/smll.202107735>.

© 2022 The Authors. Small published by Wiley-VCH GmbH. This is an open access article under the terms of the Creative Commons Attribution License, which permits use, distribution and reproduction in any medium, provided the original work is properly cited.

DOI: 10.1002/smll.202107735

### 1.1. CNT and Metastable Fluctuations: Thermodynamics and Populations

CNT is, in essence, a transition state theory,<sup>[5]</sup> which derives the standard free energy of the nucleus of critical size as a function of supersaturation by exploring the size-dependence of the surface and bulk-free energies as the two sole contributions to the nucleation's total standard free energy. Thereby, CNT categorically stipulates that the standard free energy of precritical and critical nuclei is positive. Within the CNT pseudo-equilibrium approach, this allows a useful demonstration of the associated consequences for the populations of precritical and critical nuclei. For simplicity, we assume that the standard free energy  $\Delta G^0$  of any associated (pre-critical) state is  $\Delta G^0 = 0$ , posing the formal transition between thermodynamic instability ( $\Delta G^0 > 0$ ) and stability ( $\Delta G^0 < 0$ ). Also, here, we neglect the size dependence of the standard free energy for nuclei, as opposed to CNT. Both assumptions strongly overestimate the populations. This is especially the case for larger nuclei since the standard free energy of pre-critical species increases toward a maximum characterizing the transition state, the critical nucleus, according to CNT. Regardless, within the CNT concept of unstable nuclei and the assumptions made here, the highest possible equilibrium constant  $K(\text{CNT})$  for the coexistence of these nuclei with the monomeric constituents would then be  $K(\text{CNT}) = \exp[-\Delta G^0 / RT] = \exp[0] = 1$ . Considering typical ion activity products (IAPs) of, for example, calcium carbonate pre-nucleation solutions on the order of  $5 \cdot 10^{-8}$  (supersaturation ratio  $S \approx 10$  with respect to calcite), with  $K(\text{CNT}) = 1$ , the law of mass action yields a maximally possible activity of a CNT-type, unstable nucleus consisting of one calcium and carbonate ion of roughly the same value, which is already four orders of magnitude lower than that of the single ions ( $\sqrt{5 \cdot 10^{-8}} \approx 2 \cdot 10^{-4}$ ). This shows that the reduction in activity of the monomeric ions due to CNT-type association can be readily neglected, even for an unrealistically large equilibrium constant: For typical CNT parameters, rather,  $\Delta G^0 > 0$  and  $0 < K(\text{CNT}) \ll 1$  for any precritical and critical species. Even for  $K(\text{CNT}) = 1$ , the pre-critical dimer of the CNT-ion-pair would then exist at an equilibrium activity of only circa  $(5 \cdot 10^{-8})^2 \approx 10^{-15}$ , and so forth. Since the population of larger pre-critical nuclei continues to drop exponentially, this example calculation reveals that CNT-type precursors to nucleation can hardly be ever detected experimentally—the dimers would be by far the most abundant species, being already negligible even for the unrealistically high value of  $K(\text{CNT}) = 1$ . This extrapolates to the critical nucleus. As discussed in detail elsewhere, the concentration of critical nuclei is minuscule, corresponding to—for specifically chosen, typical parameters at  $S = 10$ —one critical nucleus in a volume  $10^8$  times that of planet Earth.<sup>[13,6]</sup> While the above consideration does not allow for an assessment of the rates at which critical nuclei occur, these can be readily estimated assuming pre-exponential factors reflecting the fastest possible rearrangements in solution within an Arrhenius approach. In pseudo-equilibrium, an increase in supersaturation ratio to  $S = 20$  increases the activity of critical nuclei by 23 orders of magnitude. While this still corresponds to a negligible molar concentration, for the fastest possible rearrangement in solution, ten critical nuclei could form in  $1 \text{ mL s}^{-1}$ , thereby facilitating nucleation events. However, in a thin film

slab of the very same solution before cryo-preparation for TEM of, say,  $100 \text{ nm} \times 100 \text{ nm} \times 100 \text{ nm}$ , one critical nucleus could be observed only once in  $\approx 3$  billion years.

While the CNT expression can be parametrized to match experimental observations, and the principal dependence of nucleation rates on supersaturation and temperature is captured accurately, a priori predictions based on CNT can deviate from experimentally determined rates by many orders of magnitude.<sup>[7]</sup> Especially in protein crystallization, CNT-predictions deviate from observations, which spawned the concept of 2-step nucleation.<sup>[8,9]</sup> Initially predicted based on computer simulations,<sup>[10]</sup> this theory has been developed in great detail for protein crystallization. In essence, the metastable fluctuations first occur in terms of density (step 1), and then in terms of structure (i.e., toward ordering, step 2), and semi-empirical rate laws have been developed.<sup>[11]</sup> Here, the subdivision of one nucleation barrier into two smaller barriers can increase or decrease the overall nucleation rates as compared to CNT, and 2-step nucleation theory is therefore useful for rationalizing phenomena that occur on different time scales to those predicted by CNT. However, it is not required that the two barriers add up to the specific value of the CNT-barrier. An analogous view of 2-step nucleation is that first, (classical) nucleation of a dense liquid occurs, in which subsequently crystals nucleate at higher formal levels of supersaturation than in the mother solution. Consequently, the quantitative 2-step nucleation expressions rely on CNT.

While often termed “non-classical,” the very concept of 2-step nucleation thus relies on metastable fluctuations (in a pseudo-equilibrium perspective, that is,  $\Delta G^0 > 0$ ), and indeed, can be reconciled with CNT,<sup>[3,12]</sup> also based on CDFT approaches.<sup>[13,14]</sup> We note that especially in the protein crystallization community, these intermediate dense liquids are often referred to as “clusters.” However, according to 2-step nucleation theory, these species are considered as a nucleated phase because their formation is associated with a nucleation barrier that depends on the level of supersaturation. Herein, we thus label intermediates observed in 2-step nucleation pathways unambiguously as dense liquids. Indeed, it has been argued that 2-step nucleation theory essentially poses a parametrization of CNT so as to match experimental observations.<sup>[3]</sup> As 2-step nucleation theory relies on CNT, it cannot explain the existence of stable precursors prior to phase separation in the homogenous phase. In our opinion, the theoretical observation<sup>[13,14]</sup> of distinct relative populations of unstable pre-nucleation precursors ( $\Delta G^0 > 0$ ) in pathways resembling 2-step nucleation cannot explain the vast experimental observations of stable pre-nucleation species, as it seems impossible to rationalize *absolute* population frequencies of unstable precursors that would be sufficient for their experimental detection, and characterization (Section 1.1). However, for the dense liquid intermediates—that are formed after the first nucleation event as considered in 2-step nucleation theory—the relative heights of the barriers separating this transient state from the solution and from crystals determine their population, as is also the case for the population of amorphous particles or crystals that are metastable with respect to the final phase in CNT. In both CNT and 2-step nucleation, the barrier height toward initial nucleation depends on supersaturation, being (infinitely) high at the saturation limit, and continuously decreasing with

increasing supersaturation. Thus, 2-step nucleation and classical nucleation intermediates only form once a critical supersaturation level has been exceeded. In contrast, stable pre-nucleation clusters (PNCs) are homogeneous species that form without significant barriers in any solution state with a population given by the law of mass action and the particular standard free energy (i.e., equilibrium constant, Section 1.2).

## 1.2. Stability, Rates, and Standard Free Energy – CNT Versus PNC Pathway

As outlined in Section 1.1, standard free energies  $\Delta G^0$  and equilibrium constants  $K$  are linked via the equation (universal gas constant  $R$ , absolute temperature  $T$ )

$$\Delta G^0 = -RT \ln K \quad (1)$$

The pseudo-equilibrium approach of CNT thus relies on the very same standard state defined for equilibrium thermodynamics.<sup>3</sup> The CNT nucleation rate  $J$  is then linked to the equilibrium constant of the formation of the critical nucleus, which is assumed to be the relevant transition state<sup>[5]</sup> toward nucleation,  $K_{\text{crit}}$ , according to

$$J = AK_{\text{crit}} \quad (2)$$

The pre-factor  $A$  can also be calculated based on CNT, but the corresponding details can be neglected here. With Equation (1), this yields a kinetic law for the nucleation rate  $J$  reflecting the essence of CNT

$$J = A \exp(-\Delta G_{\text{crit}}^0 / RT) \quad (3)$$

Due to the excess surface standard free energy of precritical and critical nuclei, CNT stipulates that  $\Delta G^0(\text{CNT}) > 0$ , that is,  $0 < K(\text{CNT}) \ll 1$  (Equation (1)), where  $\Delta G_{\text{crit}}^0$  is the maximum value and a function of supersaturation. Furthermore, Equation (3) illustrates that only such unstable species are compatible with the notion of a kinetic barrier. On the contrary, the standard free energy of PNCs is negative,  $\Delta G^0(\text{PNC}) < 0$ , that is,  $K(\text{PNC}) > 1$ . For this situation, Equation (3) does not yield sensible rates, and in the non-classical theory, the barrier for phase separation originates from ongoing dehydration. Another fundamental difference between CNT-type nuclei and PNCs becomes obvious when considering the generic association equilibrium of two species  $B$  and  $C$  forming the larger species  $D$



The law of mass action defining the equilibrium constant for the formation of  $D$  from  $B$  and  $C$  is

$$K(\text{CNT or PNC}) = [D]/([B][C]) \quad (5)$$

where brackets  $[i]$  indicate equilibrium activities of species  $i$ . For  $0 < K(\text{CNT}) \ll 1$ , equilibrium 4 is (far) on the educt side if  $[i] < (1 \text{ mol/L}/c^0)$  with standard concentration  $c^0 = 1 \text{ mol L}^{-1}$ . That

is, at experimentally relevant activity products, the populations of CNT-type precritical and critical nuclei are minute, and these species can hardly be detected experimentally (Section 1.1). For  $K(\text{PNC}) > 1$ , the law of mass action (Equation (5)) does account for the shift of the equilibrium (Equation (4)) to the educt side at very low equilibrium activities of educts  $B$  and  $C$ . However, exceeding a certain activity product  $[B][C]$ , the equilibrium will shift over to the product side, and  $D$  will be more abundant than  $B$  and  $C$ . Depending on the specific value of  $K(\text{PNC})$ , which can be significantly larger than unity, this can be the case even for very low equilibrium activities of educts. The properties of equilibrium 4 thus fundamentally differ for  $K(\text{CNT})$  and  $K(\text{PNC})$ . Indeed, the quantitative PNC theory predicts the limit for association-based spontaneous phase separation from these distinct properties and  $K(\text{PNC})$ , interpreted as the liquid-liquid spinodal limit.<sup>[15]</sup> Also, the point beyond which liquid-liquid separation via monomer-association and PNCs can occur (binodal limit) can be quantitatively assessed. The agreement of theoretical and experimentally determined binodal and spinodal lines strongly suggests that the minor assumptions underlying the PNC mechanism are indeed valid for the case of calcium carbonate (Figure 3),<sup>[15]</sup> challenging the applicability of CNT for this system.

In our opinion, it is hence clear that nucleation precursor species, forming within a homogeneous phase “before phase separation”, and which are accessible to experimental characterization should be thermodynamically stable ( $\Delta G^0 < 0$ ). From the viewpoint of CNT, however, such species sit in a “free energy trap” toward nucleation, as they are energetically further away from the postulated transition state, the nucleus of critical size, than the monomeric constituents.<sup>[16]</sup> On the other hand, if nucleation precursors are thermodynamically stable, how is it even possible that they participate in phase separation processes from solutions that have become supersaturated?

One answer to this question lies in the notions of the so-called PNC pathway.<sup>[17,18]</sup> The fact that the nucleation precursors are thermodynamically stable solutes ( $\Delta G^0 < 0$ ), PNCs, is, in our opinion, what renders this pathway truly non-classical. According to CNT, monomeric solute constituents randomly collide and form unstable nuclei ( $\Delta G^0 > 0$ ) prior to reaching the critical size as the transition state (Figure 1A, top). In contrast, for the PNC pathway, the monomers associate to form thermodynamically stable ( $\Delta G^0 < 0$ ), dynamic PNCs, which are considered solutes themselves (Figure 1A, bottom). The definition of PNCs, as introduced and discussed in ref. [17] comprises five major characteristics:

- (i) PNCs are composed of the constituent atoms, molecules, or ions of a forming solid, but can also contain additional chemical species.
- (ii) PNCs are small, thermodynamically stable solutes, and there is thus formally no phase boundary between the clusters and the surrounding solution.
- (iii) PNCs are molecular precursors to the phase nucleating from solution, and hence participate in the process of phase separation.
- (iv) PNCs are highly dynamic entities, and change configuration on timescales typical for molecular rearrangements in solution (i.e., within hundreds of picoseconds).

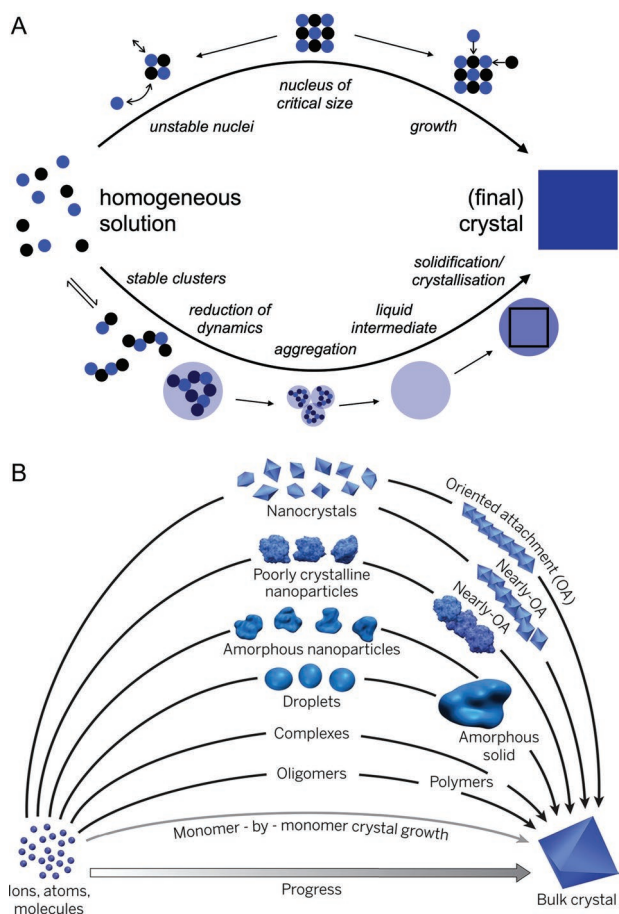


**Figure 1.** A) Schematic illustration of the basic mechanism of the onset of phase separation according to classical nucleation theory (CNT, top) and the pre-nucleation cluster (PNC) pathway (bottom). For explanation, see the text. Reproduced with minor changes under terms of the CC-BY license.<sup>[24]</sup> Copyright 2018, MDPI. B) Pathways to crystallization by particle attachment. In contrast to monomer-by-monomer addition as envisioned in classical models of crystal growth (gray curve), crystallization by particle attachment occurs by the addition of higher-order species ranging from multi-ion complexes to fully formed nanocrystals. The final faceted bulk crystal is a schematic representation of a final single-crystal state. Reproduced with permission.<sup>[1]</sup> Copyright 2015, American Association for the Advancement of Science.

(v) PNCs can have encoded structural motifs resembling, or relating to, one of the corresponding crystalline polymorphs.

That is, PNCs are part of the homogeneous solution and exhibit structural and configurational dynamics similar to other solutes. They exist in equilibrium with the various species of different sizes according to their respective standard free energies and populations given by Boltzmann statistics (law of mass action), as do nuclei according to CNT. However, due to the assumed presence of an interface, the latter are categorically associated with an excess free energy that becomes maximal at the critical size and poses the nucleation barrier, the height of which depends on the level of supersaturation. It must thus be appreciated that the properties of the association equilibria

toward a nucleus on the one hand and PNC formation on the other, in CNT and the PNC pathway, respectively, are fundamentally distinct due to the different signs of the standard free energy (Section 1.2). In the case of the PNC pathway, the event of phase separation then does not rely on overcoming a certain critical size (nucleation barrier, or level of supersaturation) as in CNT (Figure 1, top), but rather on a distinct decrease in their structural and/or configurational dynamics upon coordination or chemical changes occurring within the clusters.<sup>[17,19–22]</sup> Hereby, phase separation does not occur spontaneously from PNCs due to significant barriers associated with further dehydration.<sup>[23]</sup> This provides an answer to the above question: Stable solute clusters (PNCs) can participate in phase separation when they undergo subtle changes in structure, slowing down the cluster dynamics.<sup>[17]</sup> This event renders them a second phase, which would not be a first-order transition in the sense of Ehrenfest. That is, they change their thermodynamic speciation upon such subtle structural/chemical changes. Being stable in the homogeneous phase as solute PNCs, the phase-separated post-nucleation nanodroplets that directly emerge from the PNC precursors are then metastable with respect to amorphous or crystalline solids, but solute PNCs remain always stable in solution ( $\Delta G^0 < 0$ ). In other words, while solute PNCs are in stable equilibrium within the mother solution, as-formed post-nucleation droplets are not, since they have become a distinct phase. Driven by the as-created interfacial surface, which can be defined based on distinct dynamics in the nanodroplets and the surrounding solution and that emerges due to subtle changes in structures of PNCs, aggregative processes will yield larger liquid intermediates, which may dehydrate toward solid amorphous particles, and subsequently crystallize (Figure 1A, bottom).

It has to be noted that the existence of PNCs and the notions of the PNC pathway have been debated,<sup>[25,26]</sup> however, the raised points have been rejoindered elsewhere.<sup>[3]</sup> Indeed, one of the main arguments against PNCs, that is, that experimentally observable ion binding profiles would be inconsistent with the formation of stable multi-ion clusters, was explicitly disproven recently.<sup>[15]</sup> While the scientific soundness of theories is of course crucial, we believe that it should be pointed out that from an epistemological viewpoint, the fundamental applicability of given theories to specific problems cannot be proven or disproven in principle, and any theory should thus be judged based upon their explanatory and predictive powers. Having established the basic soundness and validity of the different nucleation theories, CNT, 2-step nucleation, and PNC pathway, herein, we consider CNT and 2-step nucleation as being classical and the PNC pathway as non-classical, as rationalized above. Considering the multitude of possible pathways from homogeneous solution to crystals, Figure 1 B does not strictly discriminate between nucleation and growth, however. For instance, nanocrystals (Figure 1B, top pathway) could be formed via a PNC pathway on one hand (Figure 1A, bottom), or via a CNT-type mechanism, that is, ion-by-ion, on the other (Figure 1A, top), and subsequently undergo oriented attachment. Any liquid or solid, amorphous or crystalline intermediate first has to be nucleated. In order to assign the specific pathway and its denomination, based on the above considerations, we propose a flow chart as illustrated in Figure 2, as best practice.



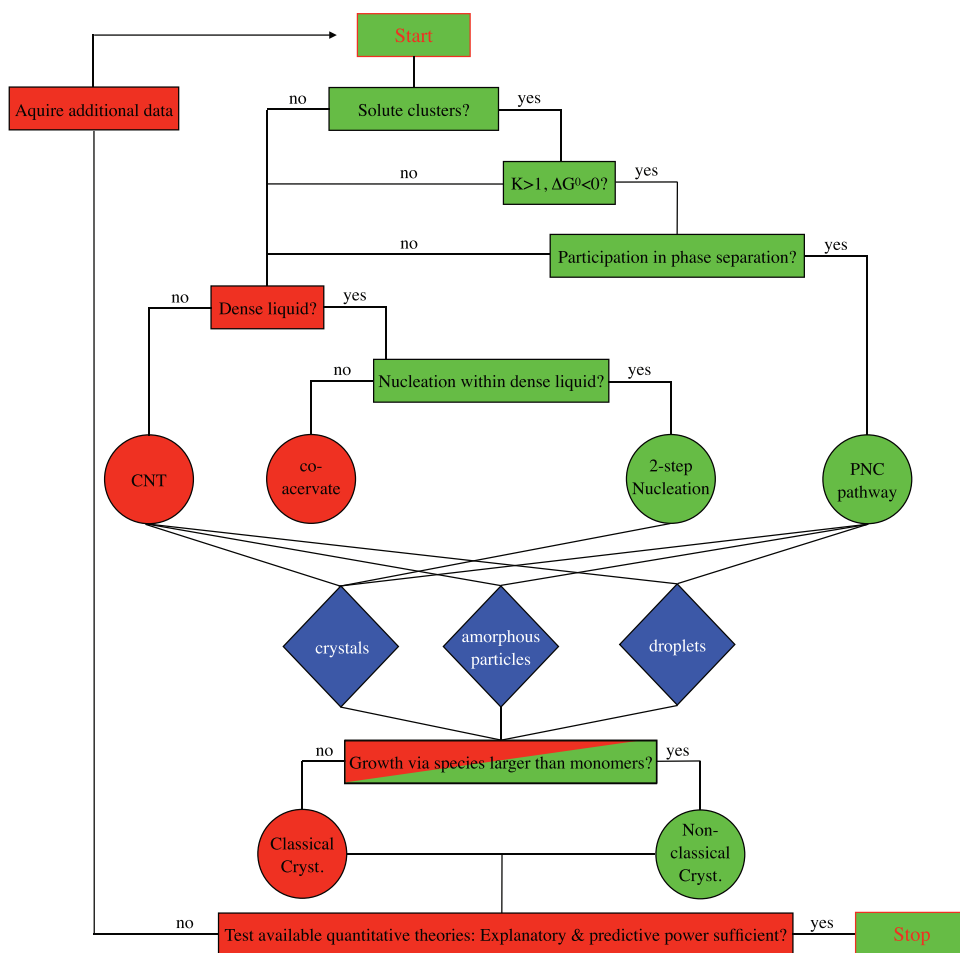


**Figure 2.** Flow scheme for the assignment of theories (circles) based on distinct experimental observations for crystallization from solution. Note that different theories can explain the emergence of liquid, amorphous, and crystalline solid phases (diamonds) in principle. For instance, it is possible that liquids are formed according to a CNT-type mechanism, although CDFT approaches suggest that this is only possible through diffusion-limited processes occurring upon unstable fluctuations (spinodal decomposition).<sup>[4,13,14]</sup> Note that the dense liquid being the intermediate in 2-step nucleation is, according to this specific theory, assumed to form via a CNT-type pathway. Thus, the PNC pathway is considered as non-classical nucleation, CNT, and 2-step nucleation as being classical (for further explanation see text). Whether or not the initially nucleated species yield larger single crystals via growth species larger than monomers then determines if the final crystallization (cryst.) process is non-classical, or not, respectively. Thus, a crystallization outcome can be obtained from a combination of non-classical nucleation and classical crystallization, for instance. Any assignment should be scrutinized against the available theoretical frameworks and, if required, re-considered. Note that several steps in the flow scheme can only be answered based on the assumption of models, the applicability of which can never be fully proven. An alternative for avoiding an infinite loop is then the parametrization of existing theories, or the development of new ones (not shown).  $K$  and  $\Delta G^0$  are the equilibrium constant and standard free energy of monomer association toward formation of clusters/nuclei in the homogeneous phase, respectively (also see Sections 1.1 and 1.2).

## 2. Recent Progress in Nucleation and Crystallization Theories

Recent progress in classical theories, such as CNT and 2-step nucleation, has been achieved through the rationalization of the mechanisms within different theoretical approaches.<sup>[13,14,27]</sup> In classical frameworks, however, the role of the solvent, water, is difficult to grasp and consider. In the PNC pathway (Figure 1A, bottom), which is initially driven by the entropy increase due to the release of hydration molecules from the monomeric solutes,<sup>[28,29]</sup> and later kinetically governed by step-wise ongoing dehydration toward the formation of bulk particles, water plays a key role. This has recently been highlighted in the case of calcium carbonate by Du and Amstad,<sup>[30]</sup> although, in our

opinion, the central role of the solvent may be the reason why non-classical nucleation could be much more general. Indeed, this critical role of the solvent creates the possibility of engineering crystallization pathways, as demonstrated for hybrid perovskites.<sup>[31]</sup> The occurrence of specific hydrated amorphous intermediates can even provide access to previously unknown crystalline (pseudo-) polymorphs.<sup>[32,33]</sup>

Sommerdijk and co-workers<sup>[34]</sup> recently introduced a novel, quantitative, kinetic model for non-classical crystallization. While the claimed initial occurrence of very small ferrihydrite nanoparticles has been challenged elsewhere,<sup>[21]</sup> due to the highly ambiguous interpretation of experimental data, this model considers the balance of colloidal forces between nanocrystals as previously proposed by Cölfen and

Antonietti,<sup>[35]</sup> and others.<sup>[36]</sup> Indeed, Ou et al.<sup>[37]</sup> used low-dose liquid-phase transmission electron microscopy (LP-TEM), particle tracking, and numerical simulations to characterize the assembly kinetics of gold nanoprisms at the single-particle level, revealing a non-classical pathway involving a dense, amorphous intermediate toward the formation of a superlattice. While both studies strictly speaking deal with post-nucleation processes, a corresponding quantitative model for the PNC pathway has been lacking.

This gap has recently been filled by the demonstration that the aqueous phase diagram of calcium carbonate can be quantitatively predicted based on the PNC model.<sup>[15]</sup> Specifically, the liquid-liquid phase diagram is quantitatively predicted based on the (measurable) thermodynamics of homogeneous phase ion association. This includes the theoretical binodal and spinodal limits of the calcium carbonate liquid-liquid miscibility gap (Figure 3), as well as the corresponding critical point, which here is located in an experimentally inaccessible region. Information on the loci of characteristic points, lines, and curves of the aqueous phase diagrams is invaluable for supporting, testing, and substantiating, for instance, the mechanistic roles of spinodal pathways toward structured single crystals,<sup>[38]</sup> or optical tweezing for controlling nucleation close to liquid-liquid critical points.<sup>[39,40]</sup> While the model allows the calculation of theoretical liquid-liquid phase diagrams based on experimentally accessible parameters, that is, essentially, with the solubilities of crystalline polymorphs and the homogeneous phase association constant as input parameters (also see Section 1.2), it is a thermodynamic model that cannot predict nucleation

rates. However, the as-formulated mechanism should allow the derivation of kinetic models, which will have to be scrutinized, just like the model of Mirabello et al.<sup>[34]</sup> in the future.

### 3. Experimental Techniques for Detection of Nucleation and Crystal Growth

Much of our recent knowledge regarding nucleation and crystal growth results from significant developments of several in situ high-resolution solution analytical techniques in recent years. They all access different aspects of the general experimental detection problem, which must be solved when looking at nucleation and early growth stages in solution:

1. Very small species starting on the atomic scale
2. Chemical reactions in the (pre)nucleation and growth process
3. High dynamics and fast processes
4. Importance of multiple species—especially in multi-step processes—so that size and shape distributions are critical

To date, no experimental technique can address all of the above characteristics, but a combination of techniques can draw a rather complete picture of the complex processes involved in nucleation and growth. Very small species (point 1) can be visualized with Liquid Phase Transmission Electron Microscopy (LP-TEM) or on surfaces by in situ atomic force microscopy (AFM), the latter also offering the determination of nucleation and growth kinetics.

For the detection of chemical reactions (point 2), X-ray based spectroscopies, like extended X-ray absorption fine structure (EXAFS) or X-ray absorption near edge spectroscopy (XANES), are suitable methods to detect the local environment around elements of interest, plus oxidation states or chemical bond formation/breakage.<sup>[44]</sup> Pair distribution function (PDF) analysis can further reveal valuable quantitative information on bond lengths. Examples include Au nanoparticle nucleation,<sup>[45]</sup> Pt synthesis from  $\text{H}_2\text{PtCl}_6 \cdot 3\text{H}_2\text{O}$ ,<sup>[46]</sup> and rod-shaped  $\text{CaSO}_4$  clusters.<sup>[47]</sup> Therefore, time-resolved EXAFS, XANES, and PDF analyses are valuable tools for the chemical and structural study of (pre)nucleation and early growth species.

Besides the above sophisticated and usually synchrotron-based techniques, simple UV-vis spectroscopy can yield valuable information if coupled to SAXS/WAXS<sup>[48,49]</sup> or analytical ultracentrifugation (AUC)<sup>[50]</sup> if suitable chromophores are present. This is particularly useful for the investigation of the early stages of semiconductor/metal nanoparticle nucleation and growth since UV/Vis spectra contain information about size, shape, crystallinity, and chemical information.<sup>[49]</sup> For ion-based reactions, ion-selective and/or conductivity electrodes are suitable for time-resolved speciation of the reacting compounds.<sup>[51]</sup>

2D solid-state Nuclear Magnetic Resonance (NMR) experiments are very useful to characterize non-classical growth processes in complex multicomponent mixtures. This was demonstrated for aragonite crystal growth via amorphous calcium carbonate (ACC) particles in corals.<sup>[52]</sup> In addition, classical NMR experiments proved useful to study the kinetics of crystallization via amorphous precursors.<sup>[53]</sup> Hyperpolarized NMR

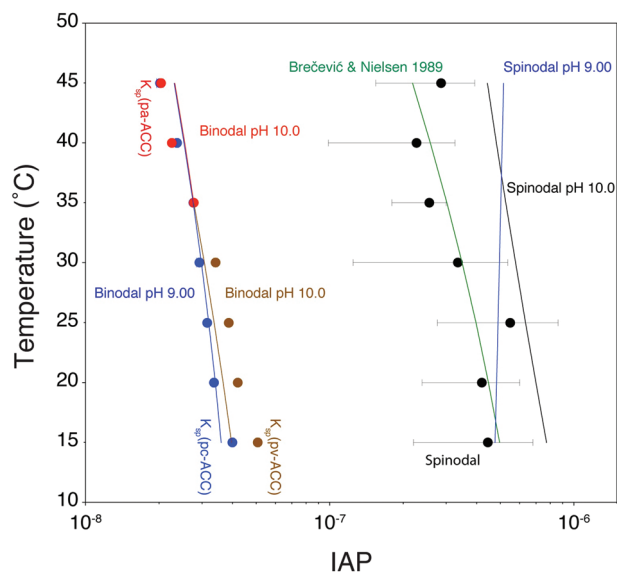


**Figure 3.** Comparison of theoretical binodal and spinodal limits defining the liquid-liquid phase diagram of the aqueous calcium carbonate system (lines) based on the quantitative PNC model with experimentally determined points (filled circles). IAP is the ion activity product. The PNC pathway-based model accounts for the experimentally observed amorphous polymorphism<sup>[41,42]</sup> in the binodal limit, and rationalizes the commonly accepted literature value of the solubility of amorphous calcium carbonate prepared from high supersaturation<sup>[43]</sup> as the corresponding spinodal limit. Reproduced under terms of the CC-BY license.<sup>[15]</sup> Copyright 2020, Wiley.

techniques may enhance the sensitivity of measurements in dilute solutions significantly,<sup>[54]</sup> and the advancement of these techniques may allow an improved understanding of solution precursors and nucleation mechanisms in the near future.

Small angle X-ray diffraction (SAXS) can detect particle sizes as an average, and even a particle size distribution if a model is assumed, with time resolution down to the  $\mu\text{s}$  domain if a free reactant jet is used<sup>[55]</sup> (point 3). Wide-angle data on crystal structures can be simultaneously determined. For a reactant jet of mixed  $\text{Cd}^{2+}$  and  $\text{S}^{2-}$  ion solutions, PNCs as growth units in a non-classical nucleation/crystallization process were revealed.<sup>[55]</sup> Gypsum was found by SAXS (time resolution 1–30 s) to grow via a four-stage process via formation and aggregation of <3 nm primary species and final crystallization to gypsum through structural rearrangement.<sup>[56]</sup> A similar scenario was found for bassanite by SAXS/WAXS with 1s time resolution.<sup>[57]</sup> In the future, the time resolution of SAXS/WAXS can be tremendously increased by the application of free electron lasers (FELs), which can produce pulses of 50 fs having as many photons as a synchrotron beam in 1 s, allowing imaging of matter at atomic resolution. Examples of FEL applications, including research on clusters, have been reviewed.<sup>[58]</sup>

In contrast, Analytical Ultracentrifugation (AUC) is a slow technique but has extremely high particle size resolution in the Ångström range<sup>[59]</sup> and can detect species down to single ions or molecules.<sup>[60]</sup> Both, SAXS and AUC detect all species in the sample to a very high level of statistical significance, while AFM and LP-TEM can only observe a few species but can image them. For slower reactions in solution, combinations of LP-TEM, AUC, titration speciation, SAXS/WAXS, EXAFS, XANES can yield the required information. Snapshots of the reaction products can be imaged by cryo-TEM. This has been successfully used to image the nucleation and early growth stages of the protein glucose isomerase via oriented attachment of clusters or nanorods at molecular resolution.<sup>[61]</sup> Another example is the crystallization of ferritin involving amorphous precursors that undergo desolvation, leading to a structural evolution toward a final crystalline phase, which arises gradually via a continuous increase in order and density.<sup>[62]</sup> For complex hybrid systems, like nucleation of inorganic particles within an organic matrix, a combination of LP-TEM, SAXS, WAXS, and AUC can characterize the system.

Another possibility to monitor fast reactions is by AUC. Here, a special synthetic boundary cell is used where one reactant solution can be overlaid onto the second forming a narrow well-defined reaction zone as introduced for the investigation of CdS formation.<sup>[63]</sup> The beauty of this method is that within a few seconds the overlaid reactant is consumed and the formed species quenched, separated, and characterized with an UV-vis spectrometer for detection of each compound's spectra.<sup>[64]</sup> Ag nucleation showed 8 species with different sizes, whose individual spectral information was determined separately.<sup>[65]</sup> Seven species in the size range 0.4–0.6 nm (corresponding to only 1–5 Ag-atoms) were found together with their UV-vis spectra probing the atomic scale. This is unsurpassed size resolution, though it requires knowledge of the particle density. However, if the diffusion coefficient distribution is determined simultaneously with the sedimentation coefficient distribution, the density of each species can then be determined, along with

size, molar mass, number of atoms in the particle core, and number of stabilizer molecules.<sup>[66]</sup> Thus, AUC can be used for the entire characterization of nanoparticles in nucleation and early growth processes even for complex multicomponent mixtures (point 4). In addition, frictional ratios of each species can be calculated, which are connected to the shape and hydration/solvation of the particles.<sup>[67]</sup> If either of these properties is known then the other can be deduced, making it a valuable tool for hydrated species, especially given the important role of water in (pre)nucleation processes.

In situ liquid phase TEM (LP-TEM) is another useful method for the investigation of small species.<sup>[68]</sup> It was used to image the nucleation of Au nanoparticles, showing the fluctuations of forming and dissolving particles,<sup>[69]</sup> which we think suggests a non-classical stable speciation, because metastable nuclei considered within CNT should be ultimately rare species (Sections 1.1 and 1.2).<sup>[3]</sup> On the other hand, if already nucleated, these species could be 2-step dense liquid intermediates as well. LP-TEM reports also exist for the formation of gold nanoparticles via spinodal decomposition of the precursor solution and nucleation of amorphous nanoclusters in the metal-rich liquid phase before crystallization of the clusters.<sup>[70]</sup> Also, Au nanoparticles were observed to nucleate secondary particles in the interfacial region  $\approx 1$  nm from their surface, which then attach to the primary nanoparticles showing that Au nucleation and growth can be a complex non-classical process.<sup>[71]</sup>

Multi-step nucleation was also observed for  $\text{CaCO}_3$  in LP-TEM and the authors suggested that the term amorphous calcium carbonate refers to a spectrum of structures ranging from the dense liquid phase to the anhydrous form,<sup>[72]</sup> consistent with the recently determined aqueous phase diagram.<sup>[15]</sup> Also, recent LP-TEM work that introduced a novel technique for mixing solutions inside of the microscope, allowed capturing the ripening process of dense liquid  $\text{CaCO}_3$  droplets formed upon spinodal decomposition, toward their binodal composition.<sup>[73]</sup> The observations appear to be in line with previous seminal work on the growth of ACC formed upon spinodal decomposition, where a monomer addition mechanism was found,<sup>[74]</sup> albeit no clear statement about the nature of the monomers was previously possible, and it seems now clear that they correspond to clusters rather than single ions. LP-TEM approaches can be extended to nucleation and growth of  $\text{CaCO}_3$  in an immobilized matrix of poly(styrene sulfonate) as interacting polymer and ion sponge, demonstrating that the technique can also be applied to hybrid systems.<sup>[75]</sup>

The capability of LP-TEM to detect lattice fringes is especially useful when detecting non-classical growth processes by oriented attachment (OA), as demonstrated for ferrihydrite nanoparticles (Figure 4-3).<sup>[76]</sup> The advantage of LP-TEM is the possibility of imaging with very high resolution, the identification of spatially-resolved crystalline and amorphous phases, and also the possibility to investigate nucleation and growth within an organic matrix, which is particularly relevant to fields like biomineralization.<sup>[75]</sup> However, a general disadvantage of LP-TEM is that high resolution comes at the cost of poor statistics since only a few particles can be observed in an experiment such that many experiments are required for a statistically relevant data set. There are also technical challenges and artifacts in LP-TEM, including heating of the sample, beam damage,

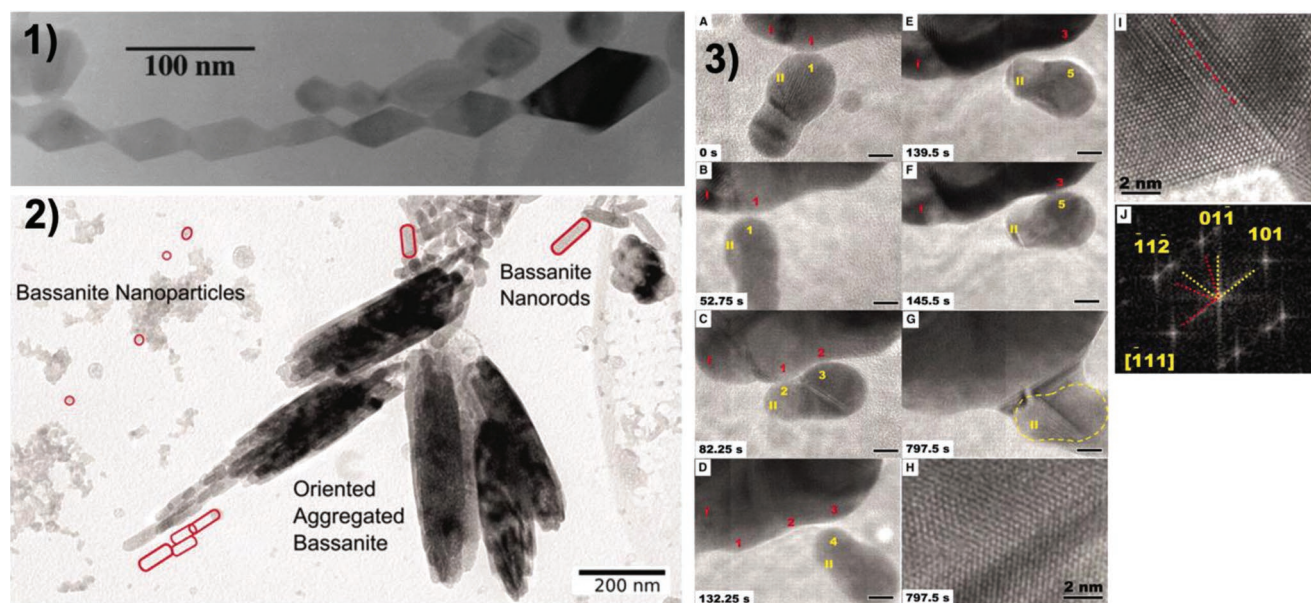


**Figure 4.** 1) TEM micrograph of a single crystal of anatase  $\text{TiO}_2$  that was hydrothermally coarsened in 0.001 M HCl. Reproduced with permission.<sup>[79]</sup> Copyright 1999, Elsevier. 2) HR-TEM micrographs of oriented bassanite ( $\text{CaSO}_4 \cdot 0.5 \text{H}_2\text{O}$ ) aggregates coexisting with individual bassanite nanorods and bassanite nanoparticles (30 s, 100 mM). Some of the single and co-oriented nanorods are decorated with red ellipsoids for ease of viewing; bassanite nanoparticles are circled in red to highlight their position (not their size). Reproduced with permission.<sup>[80]</sup> Copyright 2012, American Association for the Advancement of Science. 3) LP-TEM A–G) sequence of images showing typical dynamics of the attachment process of iron oxide ( $5\text{Fe}_2\text{O}_3 \cdot 9\text{H}_2\text{O}$ ) nanoparticles. The surfaces of particles I and II made transient contact at many points and orientations (points 1-1, 1-2, 2-3, and 3-4) before finally attaching and growing together (points 3-5). H) High-resolution image of interface in (G) showing twin structure (an inclined twin plane). The yellow dashed line in (G) shows the original boundary of the attached particle. High-resolution I) in situ TEM image and J) fast Fourier transform (FFT) of an interface from another OA event demonstrating formation of a (101) twin interface after attachment. The grain boundary is delineated by a dashed line in (I). Scale bars are 5 nm for (A–G). Reproduced with permission.<sup>[76]</sup> Copyright 2012, American Association for the Advancement of Science.

water-beam interactions, change of reactant solution chemistry as documented in the literature,<sup>[77]</sup> some of which can be overcome.<sup>[78]</sup> Given this, LP-TEM results should be considered with care.

Remarkable high-resolution insights into nucleation mechanisms are also possible with a standard (HR)TEM setup to image snapshots during a non-classical crystallization reaction and to learn about the crystallization mechanism as demonstrated for anatase  $\text{TiO}_2$  (Figure 4-1)<sup>[79]</sup> and bassanite  $\text{CaSO}_4 \cdot 0.5 \text{H}_2\text{O}$  (Figure 4-2).<sup>[80]</sup> For such snapshots, the application of cryo-TEM is beneficial to avoid drying artifacts.<sup>[62]</sup>

In situ AFM can also provide structural detail, as well as growth step velocities, and with this, thermodynamic and kinetic parameters of nucleation and growth, including in the presence of additives.<sup>[68,81,82]</sup> For large molecules like proteins, crystallization dynamics and pathways of 2D protein crystallization can be observed with single-molecule resolution.<sup>[83,84]</sup> However, a problem of AFM is the scanning speed either limiting the frame rate of observation or the spatial window. Recent advances in frequency-modulated AFM (FM-AFM) now allow for atomic resolution on surfaces for small building units even in liquid, as demonstrated for the examples of brookite  $\text{TiO}_2$ ,<sup>[85]</sup> calcite,<sup>[86,87]</sup> or NaCl.<sup>[88]</sup>

A combination of the methods discussed above would unite their strengths; the high time resolution of free jet SAXS/WAXS, vibrational and diffusive dynamics of water and other atomic constituents by combined inelastic incoherent neutron scattering and X-ray photon correlation spectroscopy,<sup>[89]</sup> high

particle size resolution of AUC, imaging, diffraction and element detection in LP-TEM, chemical speciation in EXAFS/XANES/titration and atomic surface resolution, incl. hydration layers and growth kinetics, from in situ AFM. Thus a combined approach would compensate for the disadvantages of each technique.

#### 4. Computational Approaches and Developments

Given the challenges facing experimental techniques highlighted above, one of the hopes is that both insight and even quantitative data can be obtained from the expanding arsenal of computational methods. Crystal growth and dissolution have been simulated digitally for more than half a century,<sup>[90]</sup> as the solid-liquid interface can be readily described via a grid of surface sites that can capture features such as terraces, steps, and kinks. Rates for addition to, or loss from, sites can then be determined by fitting experimental data, theoretical considerations, or from more detailed simulations.<sup>[91]</sup> While historically such models were usually applied to one surface at a time (2D), full 3D simulations of crystallization (i.e., for a whole crystal) are now also possible using either kinetic Monte Carlo<sup>[92]</sup> or simpler, more widely applicable approaches that consider the chemical potential difference between species in solution and the material as a function of saturation state.<sup>[93]</sup>

Crystallization processes occurring in solution, preceded by or upon phase-separation and nucleation, require different



modelling approaches that avoid the a priori assumption of a crystal structure. Here methods such as CDFT and phase field,<sup>[94]</sup> which describe the probability of finding species at some point in space, are very powerful due to their ability to address the potentially large length-scales that can arise. Recently, there has been an elegant demonstration that CDFT can even predict crystallization processes down to the atomic level, such as the two-step nucleation of a Lennard-Jones crystal,<sup>[13]</sup> in accord with earlier atomistic simulations.<sup>[95]</sup> While this approach has considerable promise for many systems, the application to ionic materials crystallizing from aqueous solution may prove to be a challenge. This is because the implicit treatment of water may not accurately capture the unique features of this solvent to polarize, solvate, screen, and become strongly localized around ions.

For exploring speciation and pre-nucleation cluster formation in water, where the solvent is an integral and dynamic participant in the structure, this predominantly requires atomistic techniques, such as molecular dynamics or Monte Carlo simulation, where, in the former case, both the thermodynamics and time evolution of properties can, in principle, be probed. This approach has had numerous successes in the field of crystallization, including the prediction of two-step nucleation for proteins based on a Lennard-Jones model.<sup>[10]</sup> A detailed review of the application of molecular dynamics to crystallization from liquids in general can be found elsewhere<sup>[96]</sup> and so here we focus on minerals and aqueous solution. In this context, it is important to recognize that there are limitations to the approach: Even with current petascale computing resources, such simulations are typically limited to less than a microsecond when using interatomic potentials or below a nanosecond for ab initio quantum mechanics. Neither timescale is sufficient to extract a meaningful unbiased free energy landscape for the aqueous crystallization of minerals, where interactions are stronger and the dynamics of water reorganization slower than for Lennard-Jones models, which are often considered. Therefore, aside from the quality of the underlying forces, the result of a simulation is only as good as the choice of assumed reaction coordinates used to accelerate the exploration of the dynamics via an appropriate rare-event method, thereby obtaining a low dimensional cross section through a complex free energy landscape.

An illustration of the strengths and weaknesses of theoretical methods to interrogate an experimental hypothesis comes from the speciation of calcium phosphate. Here Habraken et al.<sup>[12]</sup> proposed a pathway that includes triangular  $[\text{Ca}(\text{HPO}_4)_3]^{4-}$  complexes that aggregate via two hydrogen bonds between anions to form dimers, and beyond. Support was claimed from ab initio calculations, though being based on optimization with limited hydration, the result was irretrievably biased by the starting structure. Subsequently, there have been several further theoretical attempts to examine the plausibility of this pathway. Mancardi et al.<sup>[97]</sup> examined the free energy to remove successive ligands from the calcium tris-hydrogen phosphate complex using ab initio molecular dynamics and claimed support for the experimental Ca:P ratio of 1:3. However, the high computational cost meant that only a 3 Å range for Ca-P distances could be explored, and then only with samples of 5 picoseconds for each region; far less than the time required for water to equilibrate. Consequently, few

conclusions can be drawn regarding the standard state dissociation thermodynamics. By using more extensive simulations, Yang et al.<sup>[98]</sup> were able to map free energy profiles for a range of ion association processes, suggesting that binding was generally strongly favorable. Unfortunately, there was no attempt to extract the equilibrium constants required to quantify the speciation, while the use of a generic force field for organics was found to overbind for ion pairs relative to experimental data. Most recently, Garcia et al.<sup>[99]</sup> used multiple reaction coordinates to ensure well-converged thermodynamics for both monomeric and dimeric calcium hydrogen phosphate species. These results suggest that the  $\text{Ca}(\text{HPO}_4)_3^{4-}$  complex has a negligible concentration under the experimental conditions.<sup>[12]</sup> Furthermore, dimerization was found to occur by direct bridging of up to 3 hydrogen phosphate ions between the two calcium ions, with a stable Ca:P ratio of 1:2, shown in **Figure 5**. This demonstrates that theory does indeed have the potential to inform and even revise the pathways for pre-nucleation ion association. However, there are many pitfalls due to the challenge of fully sampling the correct thermodynamic pathway, especially when water exchange is slow on a simulation timescale. Equally important, and also often overlooked, is the need to address the fact that the configurational entropy of both the solvent and associating species is a major contributor to the free energy. Given that this depends on the available volume being sampled within the simulation cell, it is critical that the thermodynamics obtained is properly referenced to the appropriate standard state. In simulations where the explicit dissociation of species is examined, this can be achieved, for example, by aligning the free energy curve as a function of distance with the known analytic asymptotic limit for the configurational entropy.

A further cautionary tale for theoretical calculations comes from the speciation of calcium carbonate in aqueous

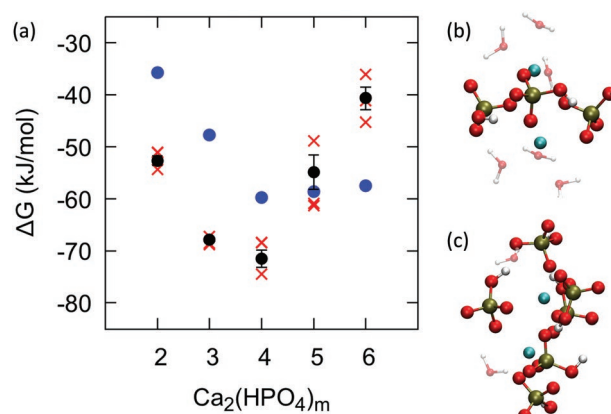


**Figure 5.** Structure and stability of pre-nucleation species in the calcium hydrogen phosphate system. a) A plot of free energy as a function of the number of ligands,  $m$ , bound to a calcium dimer is shown, where the dimer species (black circles) is more stable than the sum of the monomer free energies (blue circles) until a Ca:P ratio of 1:2 is reached (red crosses represent individual data points averaged for the dimers to show the statistical uncertainty). Structures taken from the stable free energy basin for dimers with b) 3 or c) 5  $\text{HPO}_4^{2-}$  ligands are shown illustrating that the anions directly bridge the  $\text{Ca}^{2+}$  ions. Reproduced under terms of the CC-BY license.<sup>[99]</sup> Copyright 2019, American Chemical Society.

solution. Here the quest for accurate thermodynamics has led to a range of simulations being applied to ion pairing (and beyond), from ab initio techniques through to polarizable or simpler force field models.<sup>[26,100,101]</sup> While the current quantum mechanical results can only probe the transition from the contact ion pair to the solvent-shared state with sufficient statistics, this is enough to highlight discrepancies between the different models and even between two sets of ab initio molecular dynamics at similar levels of theory. Naturally, the assumption is to place one's faith in quantum mechanics over force fields. However, it turns out that this case is an exception. Most ab initio molecular dynamics to date has, out of computational necessity, been performed with the simpler forms of DFT. Unfortunately, a known weakness is the failure to fully localize charge,<sup>[102]</sup> which is a critical problem for multiply charged anions, such as  $\text{CO}_3^{2-}$ . As a result, more accurate ab initio methods are required to correctly describe ion pairing in this system,<sup>[103]</sup> where the effective charge of the ion can strongly perturb the thermodynamics. In addition, processes such as ion pairing are often driven by the positive entropy of association due to loss of coordinated water, as is the case for calcium carbonate.<sup>[28]</sup> Hence accurate sampling of the entropy change, including that of the solvent, is as important as the more localized internal energy contribution; something that can be reliably achieved with a good force field.

A final challenge for simulations of crystallization to highlight is that of fidelity to experimental conditions. The majority of simulations are performed in ensembles with constant particle number (e.g., NVT, NPT), which implies that as crystallization progresses, the supersaturation of the solution will rapidly fall in an unrealistic manner due to the small volume of solution being simulated. Recent work<sup>[104]</sup> in applying constant chemical potential methods to the nucleation of NaCl from water suggests that this new approach (CμMD)<sup>[105]</sup> can lead to more realistic simulations.

## 5. The Role of Water at Interfaces

So far the role of water in controlling crystallization has been highlighted based on the entropic contribution to the thermodynamics and structural incorporation in species, as well as in the kinetics of stepwise dehydration of PNCs toward liquid and solid amorphous intermediates, and later, crystals. Interestingly, in case of the incorporation of magnesium ions into ACC, the higher hydration may facilitate amorphous-to-crystalline transitions within the bulk solid.<sup>[106]</sup> However, a further key influence of water is as a potential inhibitor to surface adsorption and growth, including oriented attachment. This occurs both kinetically via the rate of water exchange at a given site and in some cases via thermodynamic preference. An extensive review of water at interfaces for many systems, such as metals, oxides, ice, and liquids, can be found elsewhere.<sup>[107]</sup> Here we highlight the further example of water interfaces for biominerals. An example, par excellence, is the dominant basal surface of calcite, due to the ability to cleave large areas of clean, well-ordered terrace, making it particularly amenable to multiple experimental techniques, including X-ray reflectivity,<sup>[108]</sup> AFM,

and simulation,<sup>[109]</sup> all of which show the existence of at least two or more ordered layers of water at the interface. Indeed, such is the sensitivity of FM-AFM, it appears to image up to five hydration layers and can even identify point defects in a calcite surface via their influence on interfacial water.<sup>[110]</sup> While X-ray reflectivity typically yields just the 1-D density profile normal to the surface, it has recently been possible to fit the full 3-D distribution of water over calcite, thereby offering more detailed information against which to benchmark simulation approaches.<sup>[111]</sup>

Although the two layers of water that coordinate directly to the calcite surface are far from "ice-like," as water exchange occurs every  $\approx 2$  ns, which is only one order of magnitude slower than  $\text{Ca}^{2+}$  in solution,<sup>[112]</sup> they create a low density layer that separates them from bulk water. This unusual region actually gives rise to most of the apparent properties of this calcite surface, acting as the stable adsorption site for molecules with hydrophobic regions<sup>[113]</sup> and can even be responsible for heterogeneous nucleation, at least for liquid droplets or gas bubbles.<sup>[114]</sup> To date there is little evidence that any species exhibits sufficient thermodynamic driving force to penetrate these two water layers on a non-defective surface at neutral pH or above. While there are numerous simulations that give results for direct surface binding on calcite terraces, this is often the result of inadequate sampling of the free energy landscape (i.e., often the molecule was pre-adsorbed prior to the introduction of water). In contrast to the flat surface, stable adsorption of the carbonate anion, but not  $\text{Ca}^{2+}$ , can occur at acute or obtuse steps, though preferentially at the upper edge pointing into solution, rather than at sites that would propagate the crystal structure.<sup>[115]</sup> Again, water exchange rates are an important influence, varying by up to two orders of magnitude between different sites at steps.

In the standard model for ion-by-ion growth of surfaces, diffusion effects play a key role. Adapted from solid-gas phase interfaces, it is widely assumed that adsorption on terraces is a precursor to growth since 2D diffusion of ions across the surface is likely to provide a greater flux of species than direct collision with steps and ultimately kinks. The presence of structured water layers, leading to weak or no terrace adsorption, suggests that diffusion limitations may be more significant for such surfaces.

Sum frequency generation (SFG) and second harmonic generation (SHG) are techniques that are very sensitive to the characterization of water molecules at surfaces since they are directly able to measure interfacial water alignment.<sup>[116]</sup> The role of water in nucleation and early growth stages has so far only scarcely been investigated by these powerful techniques. Studies to date report the surface melting of ice in bilayers,<sup>[117]</sup> ice-like structuring of water by anti-freeze proteins<sup>[118]</sup> that ice-active sites within bacteria feature unique hydrophilic-hydrophobic patterns to enhance ice nucleation<sup>[119]</sup> and the formation of  $\text{CaCO}_3$  PNCs at the interface of a sea urchin biomineralization protein perturbing the structure of water.<sup>[120]</sup> Water at mineral surfaces has also been successfully characterized with high resolution on mica.<sup>[121]</sup> These few results already show that much can be learned regarding the role of water in nucleation and growth and that these techniques have considerable potential.

## 6. Conclusion

The last decade, and especially the last 5 years, have seen many exciting developments in the field of crystallization with the emergence of a diverse range of mechanistic possibilities due to our ability to probe systems in greater detail and increasingly under in situ conditions. This does not only concern inorganic ionic building units in water as we highlight in this article but also organic molecules and systems like MOFs and COFs in organic solvents as recently summarized by Li et al.<sup>[122]</sup> While many challenges remain in order to build a comprehensive rationalization of recent observations, there is good reason to be optimistic based on the new theories and techniques highlighted in the preceding sections.

Previously we have highlighted the difficulties of directly applying more rigorous quantum mechanical techniques to problems in crystallization, especially where the solvent configuration plays a critical role. Hence the prospects for the future might appear grim as growth in computer power alone will not provide a rapid solution. However, there is actually good reason to be optimistic: A recent explosion in the use of machine learning approaches has demonstrated that it is possible to reproduce the energetics of more sophisticated quantum mechanical methods at the same order of magnitude cost as for a force field. Indeed this has already been applied to the non-trivial case of the liquid properties and phase diagram of water.<sup>[123,124]</sup> Given a sufficiently comprehensive training set, this even opens up the possibility of including reactivity in such simulations at low cost. Proton transfer reactions are a natural part of mineral precursor speciation, as bicarbonate or hydrogen phosphate increasingly transforms to carbonate and phosphate, respectively, with growing cluster size. All of this could be seamlessly included, as has already been shown in an examination of proton transfer mechanisms at the oxide-water interface.<sup>[125]</sup>

Of course the power of such data-driven developments is not limited to the atomic scale, with artificial neural networks also being trained to predict overall nucleation phenomena and optimize the crystallization of materials from pharmaceuticals and proteins, through to perovskites.<sup>[126]</sup> However, the real challenge is not just to be able to predict when nucleation occurs, but to understand the actual mechanism such that it can be controlled or extrapolated to new and emerging systems. A particular experimental challenge of the future lies in the verification of the notions of the different nucleation pathways (CNT, 2-step, PNC pathway), including the recently developed quantitative PNC model and the role of water. While the early stages of precipitation, as well as the mechanism of crystal growth in water, should be revisited experimentally with the help of the newly available (high resolution) techniques, the unification of theory and experiment will be critical to progress. The utilization of cutting edge techniques with high spatial and temporal resolution as shown in **Figure 6**, keeping in mind the important role of water throughout all stages of crystallization, has great promise to advance our understanding of non-classical processes. In particular, global analysis approaches are promising, which combine data sets from different techniques in one analysis run, thus enhancing the strengths of each method for the result. For nucleation and growth, combination of the high time resolution of SAXS with the high size resolution of AUC in global analysis

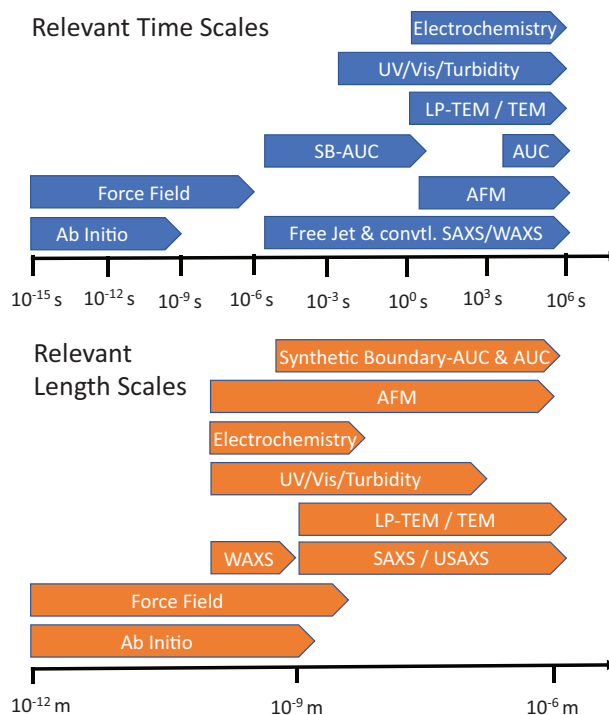


**Figure 6.** Relevant time and length scales of the theoretical and experimental methods discussed in this work. The experimental time scales can extend to long times by taking time-dependent samples. The theoretical methods can extend to lower time and length scales than shown, as well as indirectly to longer times in a small number of reaction coordinates.

is considered particularly useful. As highlighted in this review, we hope that future research will particularly engage in the combination of different experimental techniques, and quantitative simulation, so as to avoid the misinterpretation of data.

## Acknowledgements

The authors acknowledge the Deutsche Forschungsgemeinschaft (DFG) for generous financial support of their collaborative work through SFB 1214 (D.G. projects A2 & A7, J.D.G. as visiting scientist, H.C. projects B1, B3 & B6). J.D.G. thanks the Australian Research Council for funding under grant FL180100087. H.C. thanks Dr. Hao Lu, MPI for Polymer Research, Mainz for discussion on SFG/SHG techniques and cooperation.

Open access funding enabled and organized by Projekt DEAL.

## Conflict of Interest

The authors declare no conflict of interest.

## Keywords

2-step nucleation, classical nucleation theory, crystal growth, pre-nucleation clusters, water

Received: March 8, 2022

Revised: May 7, 2022

Published online: June 9, 2022

- [1] J. J. De Yoreo, P. U. P. A. Gilbert, N. A. J. M. Sommerdijk, R. L. Penn, S. Whitelam, D. Joester, H. Zhang, J. D. Rimer, A. Navrotsky, J. F. Banfield, A. F. Wallace, F. M. Michel, F. C. Meldrum, H. Cölfen, P. M. Dove, *Science* **2015**, 349, aaa6760.
- [2] J. J. De Yoreo, P. G. Vekilov, *Rev. Mineral. Geochem.* **2003**, 54, 57.
- [3] D. Gebauer, P. Raiteri, J. D. Gale, H. Cölfen, *Am. J. Sci* **2018**, 318, 969.
- [4] J. W. Cahn, J. E. Hilliard, *J. Chem. Phys.* **1959**, 31, 688.
- [5] H. Eyring, *Chem. Rev.* **1935**, 17, 65.
- [6] A. E. Nielsen, *Kinetics of Precipitation*, Pergamon Press, New York **1964**.
- [7] P. G. Vekilov, *Cryst. Growth Des.* **2010**, 10, 5007.
- [8] P. G. Vekilov, *Cryst. Growth Des.* **2004**, 4, 671.
- [9] P. G. Vekilov, *Nanoscale* **2010**, 2, 2346.
- [10] P. R. ten Wolde, D. Frenkel, *Science* **1997**, 277, 1975.
- [11] W. Pan, A. B. Kolomeisky, P. G. Vekilov, *J. Chem. Phys.* **2005**, 122, 174905.
- [12] W. J. E. M. Habraken, J. Tao, L. J. Brylka, H. Friedrich, L. Bertinetti, A. S. Schenk, A. Verch, V. Dmitrovic, P. H. H. Bomans, P. M. Frederik, J. Laven, P. van der Schoot, B. Aichmayer, G. de With, J. J. DeYoreo, N. A. J. M. Sommerdijk, *Nat. Commun.* **2013**, 4, 1507.
- [13] J. F. Lutsko, *Sci. Adv.* **2019**, 5, eaav7399.
- [14] M. A. Durán-Olivencia, P. Yatsyshin, S. Kalliadasis, J. F. Lutsko, *New J. Phys.* **2018**, 20, 083019.
- [15] J. T. Avaro, Wolf, S. L. P., K. Hauser, D. Gebauer, *Angew. Chem., Int. Ed.* **2020**, 59, 6155.
- [16] J. J. De Yoreo, *Nat. Mater.* **2013**, 12, 284.
- [17] D. Gebauer, M. Kellermeier, J. D. Gale, L. Bergström, H. Cölfen, *Chem. Soc. Rev.* **2014**, 43, 2348.
- [18] D. Gebauer, S. E. Wolf, *J. Am. Chem. Soc.* **2019**, 141, 4490.
- [19] A. F. Wallace, L. O. Hedges, A. Fernandez-Martinez, P. Raiteri, J. D. Gale, G. A. Waychunas, S. Whitelam, J. F. Banfield, J. J. De Yoreo, *Science* **2013**, 341, 885.
- [20] M. J. Lukić, E. Wiedenbeck, H. Reiner, D. Gebauer, *Sci. Adv.* **2020**, 6, eaba6878.
- [21] M. J. Lukić, D. Gebauer, A. Rose, *Curr. Opin. Colloid Interface Sci.* **2020**, 46, 114.
- [22] E. D. Bøjesen, B. B. Iversen, *CrystEngComm* **2016**, 18, 8332.
- [23] R. Demichelis, P. Raiteri, J. D. Gale, D. Quigley, D. Gebauer, *Nat. Commun.* **2011**, 2, 590.
- [24] D. Gebauer, *Minerals* **2018**, 8, 179.
- [25] P. J. M. Smeets, A. R. Finney, W. J. E. M. Habraken, F. Nudelman, H. Friedrich, J. Laven, J. J. De Yoreo, P. M. Rodger, N. A. J. M. Sommerdijk, *Proc. Natl. Acad. Sci. USA* **2017**, 114, E7882.
- [26] K. Henzler, E. O. Fetisov, M. Galib, M. D. Baer, B. A. Legg, C. Borca, J. M. Xto, S. Pin, J. L. Fulton, G. K. Schenter, N. Govind, J. I. Siepmann, C. J. Mundy, T. Huthwelker, J. J. De Yoreo, *Sci. Adv.* **2018**, 4, eaao6283.
- [27] D. Kashchiv, *J. Cryst. Growth* **2020**, 530, 125300.
- [28] M. Kellermeier, P. Raiteri, J. K. Berg, A. Kempter, J. D. Gale, D. Gebauer, *ChemPhysChem* **2016**, 17, 3535.
- [29] J. Scheck, L. Fuhrer, B. Wu, M. Drechsler, D. Gebauer, *Chem. - Eur. J.* **2019**, 25, 13002.
- [30] H. Du, E. Amstad, *Angew. Chem., Int. Ed.* **2020**, 59, 1798.
- [31] A. G. Ortoll-Bloch, H. C. Herbol, B. A. Sorenson, M. Poloczek, L. A. Estroff, P. Clancy, *Cryst. Growth Des.* **2019**, 20, 1162.
- [32] B.-Q. Lu, T. Willhammar, B.-B. Sun, N. Hedin, J. D. Gale, D. Gebauer, *Nat. Commun.* **2020**, 11, 3130.
- [33] Z. Zou, W. J. E. M. Habraken, G. Matveeva, A. C. S. Jensen, L. Bertinetti, M. A. Hood, C. Sun, P. U. P. A. Gilbert, I. Polishchuk, B. Pokroy, J. Mahamid, Y. Politi, S. Weiner, P. Werner, S. Bette, R. Dinnebie, U. Kolb, E. Zolotoyabko, P. Fratzl, *Science* **2019**, 363, 396.
- [34] G. Mirabello, A. Ianiro, P. H. H. Bomans, T. Yoda, A. Arakaki, H. Friedrich, G. de With, N. A. J. M. Sommerdijk, *Nat. Mater.* **2019**, 19, 391.
- [35] H. Cölfen, M. Antonietti, *Mesocrystals and Nonclassical Crystallization*, John Wiley & Sons, Chichester **2008**.
- [36] V. Nikolakis, E. Kokkoli, M. Tirrell, M. Tsapatsis, D. G. Vlachos, *Chem. Mater.* **2000**, 12, 845.
- [37] Z. Ou, Z. Wang, B. Luo, E. Luijten, Q. Chen, *Nat. Mater.* **2019**, 19, 450.
- [38] E. Seknazi, S. Kozachkevich, I. Polishchuk, N. Bianco Stein, J. Villanova, J.-P. Suuronen, C. Dejoie, P. Zaslansky, A. Katsman, B. Pokroy, *Nat. Commun.* **2019**, 10, 664.
- [39] F. Walton, K. Wynne, *Soft Matter* **2019**, 15, 8279.
- [40] F. Walton, K. Wynne, *Nat. Chem.* **2018**, 10, 506.
- [41] J. H. E. Cartwright, A. G. Checa, J. D. Gale, D. Gebauer, C. I. Sainz-Díaz, *Angew. Chem., Int. Ed.* **2012**, 51, 11960.
- [42] M. Farhadi Khouzani, D. M. Chevrier, P. Zhang, N. Hedin, D. Gebauer, *Angew. Chem., Int. Ed.* **2016**, 55, 8117.
- [43] L. Brečević, A. E. Nielsen, *J. Cryst. Growth* **1989**, 98, 504.
- [44] S. Wu, M. Li, Y. Sun, *Angew. Chem., Int. Ed.* **2019**, 58, 8987.
- [45] T. Tanaka, J. Ohyama, K. Teramura, Y. Hitomi, *Catal. Today* **2012**, 183, 108.
- [46] D. Saha, E. D. Bøjesen, K. M. Ø. Jensen, A.-C. Dippel, B. B. Iversen, *J. Phys. Chem. C* **2015**, 119, 13357.
- [47] T. M. Stawski, A. E. S. Van Driessche, R. Besselink, E. H. Byrne, P. Raiteri, J. D. Gale, L. G. Benning, *J. Phys. Chem. C* **2019**, 123, 23151.
- [48] M. Herbst, E. Hofmann, S. Förster, *Langmuir* **2019**, 35, 11702.
- [49] X. Hao, M. Chen, L. Wang, Z. Cao, Y. Li, S. Han, M. Zhang, K. Yu, J. Zeng, *Chem. Commun.* **2020**, 56, 2031.
- [50] E. Karabudak, E. Brookes, V. Lesnyak, N. Gaponik, A. Eychmüller, J. Walter, D. Segets, W. Peukert, W. Wohlleben, B. Demeler, H. Cölfen, *Angew. Chem., Int. Ed.* **2016**, 55, 11770.
- [51] M. Kellermeier, H. Cölfen, D. Gebauer, *Methods Enzymol.* **2013**, 532, 45.
- [52] S. Von Euw, Q. Zhang, V. Manichev, N. Murali, J. Gross, L. C. Feldman, T. Gustafsson, C. Flach, R. Mendelsohn, P. G. Falkowski, *Science* **2017**, 356, 933.
- [53] C. E. Hughes, P. A. Williams, B. M. Kariuki, K. D. M. Harris, *ChemPhysChem* **2018**, 19, 3341.
- [54] E. M. M. Weber, T. Kress, D. Abergel, S. Sewsurn, T. Azaïs, D. Kurzbach, *Anal. Chem.* **2020**, 92, 7666.
- [55] A. Schiener, A. Magerl, A. Krach, S. Seifert, H.-G. Steinrück, J. Zagorac, D. Zahn, R. Wehrich, *Nanoscale* **2015**, 7, 11328.
- [56] T. M. Stawski, A. E. S. Van Driessche, M. Ossorio, J. D. Rodriguez-Blanco, R. Besselink, L. G. Benning, *Nat. Commun.* **2016**, 7, 11177.
- [57] T. M. Stawski, R. Besselink, K. Chatzipanagis, J. Hövelmann, L. G. Benning, A. E. S. Van Driessche, *J. Phys. Chem. C* **2020**, 124, 8411.
- [58] J. Rossbach, J. R. Schneider, W. Wurth, *Phys. Rep.* **2019**, 808, 1.
- [59] H. Cölfen, T. Pauck, *Colloid Polym. Sci.* **1997**, 275, 175.
- [60] D. Gebauer, A. Völkel, H. Cölfen, *Science* **2008**, 322, 1819.
- [61] A. E. S. Van Driessche, N. Van Gerven, P. H. H. Bomans, R. R. M. Joosten, H. Friedrich, D. Gil-Carton, N. A. J. M. Sommerdijk, M. Sleutel, *Nature* **2018**, 556, 89.
- [62] L. Houben, H. Weissman, S. G. Wolf, B. Rybtchinski, *Nature* **2020**, 579, 540.
- [63] L. Börger, H. Cölfen, M. Antonietti, *Colloids Surf., A* **2000**, 163, 29.
- [64] J. Pearson, J. Walter, W. Peukert, H. Cölfen, *Anal. Chem.* **2017**, 90, 1280.
- [65] C. M. Schneider, H. Cölfen, *J. Phys. Chem. Lett.* **2019**, 10, 6558.
- [66] R. P. Carney, J. Y. Kim, H. Qian, R. Jin, H. Mehenni, F. Stellacci, O. M. Bakr, *Nat. Commun.* **2011**, 2, 7635.
- [67] S. E. Harding, *Biophys. Chem.* **1995**, 55, 69.



- [68] J. Tao, M. H. Nielsen, J. J. De Yoreo, *Curr. Opin. Colloid Interface Sci.* **2018**, 34, 74.
- [69] M. H. Nielsen, D. Li, H. Zhang, S. Aloni, T. Y.-J. Han, C. Frandsen, J. Seto, J. F. Banfield, H. Cölfen, J. J. De Yoreo, *Microsc. Microanal.* **2014**, 20, 425.
- [70] N. D. Loh, S. Sen, M. Bosman, S. F. Tan, J. Zhong, C. A. Nijhuis, P. Král, P. Matsudaira, U. Mirsaidov, *Nat. Chem.* **2016**, 9, 77.
- [71] Y. Cheng, J. Tao, G. Zhu, J. A. Soltis, B. A. Legg, E. Nakouzi, J. J. De Yoreo, M. L. Sushko, J. Liu, *Nanoscale* **2018**, 10, 11907.
- [72] M. H. Nielsen, S. Aloni, J. J. De Yoreo, *Science* **2014**, 345, 1158.
- [73] D. J. Kelly, N. Clark, M. Zhou, D. Gebauer, R. V. Gorbachev, S. J. Haigh, *Adv. Mater.* **2021**, 33, 2100668.
- [74] J. Liu, S. Pancera, V. Boyko, A. Shukla, T. Narayanan, K. Huber, *Langmuir* **2010**, 26, 17405.
- [75] P. J. M. Smeets, K. R. Cho, R. G. E. Kempen, N. A. J. M. Sommerdijk, J. J. De Yoreo, *Nat. Mater.* **2015**, 14, 394.
- [76] D. Li, M. H. Nielsen, J. R. I. Lee, C. Frandsen, J. F. Banfield, J. J. De Yoreo, *Science* **2012**, 336, 1014.
- [77] T. J. Woehl, K. L. Jungjohann, J. E. Evans, I. Arslan, W. D. Ristenpart, N. D. Browning, *Ultramicroscopy* **2013**, 127, 53.
- [78] G. Zhu, H. Reiner, H. Cölfen, J. J. De Yoreo, *Micron* **2019**, 118, 35.
- [79] R. L. Penn, J. F. Banfield, *Geochim. Cosmochim. Acta* **1999**, 63, 1549.
- [80] A. E. S. Van Driessche, L. G. Benning, J. D. Rodriguez-Blanco, M. Ossorio, P. Bots, J. M. García-Ruiz, *Science* **2012**, 336, 69.
- [81] C. Zeng, C. Vitale-Sullivan, X. Ma, *Minerals* **2017**, 7, 158.
- [82] M. Li, L. Wang, C. V. Putnis, *CrystEngComm* **2018**, 20, 2886.
- [83] M. Sleutel, J. Lutsko, A. E. S. Van Driessche, M. A. Durán-Olivencia, D. Maes, *Nat. Commun.* **2014**, 5, 343.
- [84] S. Chung, S. H. Shin, C. R. Bertozzi, J. J. De Yoreo, *Proc. Natl. Acad. Sci. USA* **2010**, 107, 16536.
- [85] H. Asakawa, E. Holmström, A. S. Foster, S. Kamimura, T. Ohno, T. Fukuma, *J. Phys. Chem. C* **2018**, 122, 24085.
- [86] J. Tracey, K. Miyazawa, P. Spijker, K. Miyata, B. Reischl, F. F. Canova, A. L. Rohl, T. Fukuma, A. S. Foster, *Nanotechnology* **2016**, 27, 415709.
- [87] K. Miyata, Y. Kawagoe, J. Tracey, K. Miyazawa, A. S. Foster, T. Fukuma, *J. Phys. Chem. C* **2019**, 123, 19786.
- [88] F. Ito, K. Kobayashi, P. Spijker, L. Zivanovic, K. Umeda, T. Nurmi, N. Holmberg, K. Laasonen, A. S. Foster, H. Yamada, *J. Phys. Chem. C* **2016**, 120, 19714.
- [89] A. Koishi, A. Fernandez-Martinez, B. Ruta, M. Jimenez-Ruiz, R. Poloni, D. Di Tommaso, F. Zontone, G. A. Waychunas, G. Montes-Hernandez, *J. Phys. Chem. C* **2018**, 122, 16983.
- [90] U. Bertocci, *Surf. Sci.* **1969**, 15, 286.
- [91] M. N. Joswiak, M. F. Doherty, B. Peters, *Proc. Natl. Acad. Sci. USA* **2018**, 115, 656.
- [92] S. Piana, M. Reyhani, J. D. Gale, *Nature* **2005**, 438, 70.
- [93] M. W. Anderson, J. T. Gebbie-Rayet, A. R. Hill, N. Farida, M. P. Atfield, P. Cubillas, V. A. Blatov, D. M. Proserpio, D. Akporiaye, B. Arstad, J. D. Gale, *Nature* **2017**, 544, 456.
- [94] L. Gránásy, G. I. Tóth, J. A. Warren, F. Podmaniczky, G. Tegze, L. Rátkai, T. Pusztai, *Prog. Mater. Sci.* **2019**, 106, 100569.
- [95] J. Anwar, P. K. Boateng, *J. Am. Chem. Soc.* **1998**, 120, 9600.
- [96] G. C. Sosso, J. Chen, S. J. Cox, M. Fitzner, P. Pedevilla, A. Zen, A. Michaelides, *Chem. Rev.* **2016**, 116, 7078.
- [97] G. Mancardi, U. Terranova, N. H. de Leeuw, *Cryst. Growth Des.* **2016**, 16, 3353.
- [98] X. Yang, M. Wang, Y. Yang, B. Cui, Z. Xu, X. Yang, *Phys. Chem. Chem. Phys.* **2019**, 21, 14530.
- [99] N. A. Garcia, R. I. Malini, C. L. Freeman, R. Demichelis, P. Raiteri, N. A. J. M. Sommerdijk, J. H. Harding, J. D. Gale, *Cryst. Growth Des.* **2019**, 19, 6422.
- [100] G. A. Tribello, F. Bruneval, C. Liew, M. Parrinello, *J. Phys. Chem. B* **2009**, 113, 11680.
- [101] P. Raiteri, R. Demichelis, J. D. Gale, *J. Phys. Chem. C* **2015**, 119, 24447.
- [102] E. R. Johnson, A. Otero-de-la-Roza, S. G. Dale, *J. Chem. Phys.* **2013**, 139, 184116.
- [103] P. Raiteri, A. Schuitemaker, J. D. Gale, *J. Phys. Chem. B* **2020**, 124, 3568.
- [104] T. Karmakar, P. M. Piaggi, M. Parrinello, *J. Chem. Theory Comput.* **2019**, 15, 6923.
- [105] C. Perego, M. Salvalaglio, M. Parrinello, *J. Chem. Phys.* **2015**, 142, 144113.
- [106] Z. Liu, Z. Zhang, Z. Wang, B. Jin, D. Li, J. Tao, R. Tang, J. J. De Yoreo, *Proc. Natl. Acad. Sci. USA* **2020**, 117, 3397.
- [107] O. Björneholm, M. H. Hansen, A. Hodgson, L.-M. Liu, D. T. Limmer, A. Michaelides, P. Pedevilla, J. Rossmeisl, H. Shen, G. Tocci, E. Tyrode, M.-M. Walz, J. Werner, H. Bluhm, *Chem. Rev.* **2016**, 116, 7698.
- [108] P. Fenter, N. C. Sturchio, *Prog. Surf. Sci.* **2004**, 77, 171.
- [109] P. Fenter, S. Kerisit, P. Raiteri, J. D. Gale, *J. Phys. Chem. C* **2013**, 117, 5028.
- [110] H. Söngén, B. Reischl, K. Miyata, R. Bechstein, P. Raiteri, A. L. Rohl, J. D. Gale, T. Fukuma, A. Kühnle, *Phys. Rev. Lett.* **2018**, 120, 116101.
- [111] S. J. T. Brugman, P. Raiteri, P. Accordini, F. Megens, J. D. Gale, E. Vlieg, *J. Phys. Chem. C* **2020**, 124, 18564.
- [112] M. De La Pierre, P. Raiteri, J. D. Gale, *Cryst. Growth Des.* **2016**, 16, 5907.
- [113] M. Nalbach, P. Raiteri, S. Klassen, S. Schäfer, J. D. Gale, R. Bechstein, A. Kühnle, *J. Phys. Chem. C* **2017**, 121, 24144.
- [114] A. Silvestri, E. Ataman, A. Budi, S. L. S. Stipp, J. D. Gale, P. Raiteri, *Langmuir* **2019**, 35, 16669.
- [115] M. De La Pierre, P. Raiteri, A. G. Stack, J. D. Gale, *Angew. Chem., Int. Ed.* **2017**, 56, 8464.
- [116] M. Bonn, Y. Nagata, E. H. G. Backus, *Angew. Chem., Int. Ed.* **2015**, 54, 5560.
- [117] M. A. Sánchez, T. Kling, T. Ishiyama, M.-J. van Zadel, P. J. Bisson, M. Mezger, M. N. Jochum, J. D. Cyran, W. J. Smit, H. J. Bakker, M. J. Shultz, A. Morita, D. Donadio, Y. Nagata, M. Bonn, E. H. G. Backus, *Proc. Natl. Acad. Sci. USA* **2017**, 114, 227.
- [118] K. Meister, S. Strazdaite, A. L. DeVries, S. Lotze, L. L. C. Olijve, I. K. Voets, H. J. Bakker, *Proc. Natl. Acad. Sci. USA* **2014**, 111, 17732.
- [119] R. Pandey, K. Usui, R. A. Livingstone, S. A. Fischer, J. Pfaendtner, E. H. G. Backus, Y. Nagata, J. Fröhlich-Nowoisky, L. Schmäser, S. Mauri, J. F. Scheel, D. A. Knopf, U. Pöschl, M. Bonn, T. Weidner, *Sci. Adv.* **2016**, 2, e1501630.
- [120] H. Lu, Y.-C. Huang, J. Hunger, D. Gebauer, H. Cölfen, M. Bonn, *J. Am. Chem. Soc.* **2021**, 143, 1758.
- [121] A. Tuladhar, Z. A. Chase, M. D. Baer, B. A. Legg, J. Tao, S. Zhang, A. D. Winkelman, Z. Wang, C. J. Mundy, J. J. De Yoreo, H. Wang, *J. Am. Chem. Soc.* **2019**, 141, 2135.
- [122] X. Li, J. Wang, T. Wang, N. Wang, S. Zong, X. Huang, H. Hao, *Sci. China: Chem.* **2021**, 64, 1460.
- [123] H. Wang, W. Yang, *J. Phys. Chem. Lett.* **2018**, 9, 3232.
- [124] B. Cheng, E. A. Engel, J. Behler, C. Dellago, M. Ceriotti, *Proc. Natl. Acad. Sci. USA* **2019**, 116, 1110.
- [125] V. Quaranta, M. Hellström, J. Behler, *J. Phys. Chem. Lett.* **2017**, 8, 1476.
- [126] T. Hjorth, M. Svärd, A. C. Rasmuson, *CrystEngComm* **2019**, 21, 449.



**Denis Gebauer** is professor at the Institute of Inorganic Chemistry of Leibniz University Hannover (Germany). After completing his Ph.D. at the Max-Planck-Institute of Colloids and Interfaces, he stayed at Stockholm University as postdoctoral researcher. Afterward, he became an assistant professor at the University of Konstanz. Gebauer has received various awards including a Zukunftskolleg Research Fellowship, and the Heinz Maier-Leibnitz Prize (German Research Foundation & German Ministry of Education and Research). His research focuses on mechanisms of nucleation and crystallization. The application and development of analytical techniques for answering questions in these areas is a core expertise of the Gebauer group.



**Julian D. Gale** obtained his first degree in Chemistry and his doctorate from the University of Oxford. After a postdoctoral position at the Royal Institution of Great Britain, he moved to Imperial College London as a Royal Society University research fellow and subsequently reader in Theoretical and Computational Chemistry. In 2003, he moved to Curtin University, as a Premier's research fellow and now holds the position of John Curtin Distinguished Professor of Computational Chemistry and Australian Research Council Laureate Fellow. Research interests include the development and application of computational techniques to problems in areas including materials chemistry, crystallization, and geochemistry.



**Helmut Cölfen** is a full professor of Physical Chemistry at the University of Konstanz. His research interests are in the area of nucleation, classical and non-classical crystallization, biomineralization, synthesis of functional polymers, directed self-assembly of nanoparticles and fractionating methods of polymer, and nanoparticle analysis. His group has made contributions to high resolution particle size analysis with Angström resolution in solution, mesocrystals, nonclassical nucleation and crystallization,  $\text{CaCO}_3$  crystallization, bio-inspired mineralization, synthesis of double hydrophilic block copolymers, and additive controlled crystallization. He has published more than 400 papers and was listed among the top 100 chemists 2000–2010 by Thomson Reuters.